Inverse kinematics analysis of a P2CuP2Cu concentric tube robot with embedded micro-actuation for 3T-1R tasks

Mohamed Taha Chikhaoui, Kanty Rabenorosoa, and Nicolas Andreff

Abstract This paper introduces a novel kinematic structure based on the concentric tube robot (CTR) paradigm, augmented with embedded micro-actuation. The latter allows to replace troublesome R-joints in CTR with 3 tubes by active tube curvatures (Cu-joints). First, the forward kinematic model is derived. Furthermore, the inverse kinematic problem is partially solved by restricting it to 3-translations / 1-rotation movements. Finally, the inverse model is used to perform path planning schemes in medical scenarios.

Key words: Concentric tube robot, embedded micro-actuation, path planning, medical application.

1 Introduction

Flexible and miniaturized instruments are widely used for minimally invasive interventions. In this scope, continuum robots provide doctors with a controllable small device with high precision navigation inside the human body for both therapeutic and diagnosis purposes [4]. Particularly, concentric tube robots (CTR) have proven their efficiency for a wide range of medical applications [3, 9–11, 13] . CTR are formed by several pre-shaped tubes nested in each other that can translate and rotate relatively in a telescopic way. The improved efficiency is due, among other reasons, to the use of tubes of small diameters ranging from 5mm down to 0.8mm with a free lumen able to embed different medical tools. Despite all these advantages, CTR suffer from mechanical limits such as snapping explained in [15] and caused by the high torsional energy involved when rotating the tubes relatively. In fact, the rotation input at the tube base is all the more different from its output angle at the tip

AS2M Department, FEMTO-ST Institute, UBFC/UFC/CNRS/ENSMM/UTBM.
24 rue A. Savary, Besançon, France. e-mail: mohamed.chikhaoui@femto-st.fr

as its length and/or curvature are higher. Another issue with CTR is that once their assembly is performed, the curvature of each tube is a fixed parameter and cannot be modified afterward, which narrows the possible workspace to cover as demonstrated in [7,8]. Furthermore, in order to perform the relative movements, each tube is attached to the rotation stage, which is, in most of the cases, connected to the translation stage [2, 3, 5, 9, 14, 16]. For n concentric tubes, one needs $2n$ actuators that should overcome the frictional and torsional efforts of the tubes and thus are of a consequent size compared to the effector size. With a 3-tube CTR, 6 actuators are used implying the possibility to control the 6 degrees of freedom (DoF) of the robot end-effector.

The aim of this work is to propose an equivalent structure of a standard CTR but augmented with embedded micro-actuation based on 2 tubes only and considered as a P2CuP2Cu such as P denotes the prismatic joints equivalent to the translational movements and 2 active tube curvatures in 2 orthogonal directions for each tube denoted by Cu for each bending. This structure is intended to keep the same performances with less mechanical constraints and an embedded actuation scheme able to be easily integrated into an actual operating room. If the forward kinematic model is rather easy to derive, inversion of the robot model in a geometrical way is useful for a stable path planning including obstacle avoidance, tissue and organ examination with imaging systems, and full robot shape monitoring in constrained environments. This solution is proposed here in contrast with (i) Jacobian-based inverse-kinematics that require a full knowledge of the kinematics, an important computational time and that are tributary to the non-singular configurations [9], and with (ii) the kinematic-equivalent model based inverse kinematics [12] that monitor exclusively the position of the robot tip (added to the overall shape) by solution exploration without controlling its orientation.

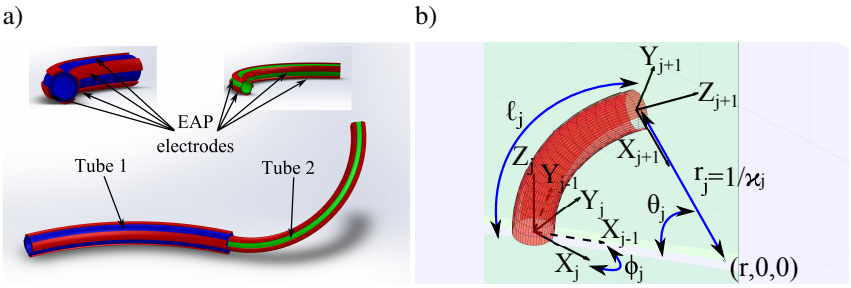

Fig. 1 a) CAD design of the proposed P2CuP2Cu robot based on embedded micro-actuators b) Schematic description of an arc of a circle in 3D where the light blue plane contains the previous section $j-1$ and the light green is the actual plane containing the section j.

For the sake of the completeness of this introduction, a few words are needed on technology. The comparison of the available micro-actuators such as shape memory alloys (SMA) and piezoelectric materials (PEM) presents the electro-active polymers (EAP) as the best candidates for this application. In fact, EAP-based actuators do not produce additional heating in contrast with SMA, require very low voltages

(<2 Volts for some ionic EAP) in contrast with PEM, and do not alter the structure mechanics because of their lightweight [7]. Biocompatibility with a medical device is also confirmed and a relatively high strain (more than 10%) should be noted. Section 2 presents the combination of these promising technologies and the forward modeling as the first work led to the best of our knowledge. Furthermore, the inversion of these models is developed in a geometrical way in section 3 for the P2CuP2Cu, and simulations of path planning results are presented based on the developed models.

2 Concentric tube robot with embedded micro-actuation

2.1 Embedded micro-actuation in concentric tube robots

Adding micro-actuation to a concentric tube robot provides several improvements. First, the intrinsic curvature of each tube is accessible when activating the EAP-based micro-actuators deposed as 4 electrodes onto each tube as described in figure 1a. In fact, each pair of electrodes generates antagonistic efforts due to an electro-chemo-mechanical conversion. When one positively activated electrode expands in volume, its diametrically opposite one (negatively activated) shrinks which leads to the bending of the substrate tube along the plane containing these electrode central lines. This emerging technology is under continuous improvement and has shown promising results that required expertise in chemistry, micro-fabrication and clean room developments [1]. Moreover, with this 4-electrodes configuration, the rotation motors are not mandatory which reduces substantially the actuation unit size. Furthermore, biocompatible flexible tubes are used and thus small efforts are required to deploy them telescopically. Smaller translation stages are adequate and replace for the high-torque-requiring motors used in CTR actuation. The thickness of such actuators varies between 10 and 30 microns and thus does not alter the concentric tube approach and saves the free-lumen configuration, in contrast with cable-driven continuum robots [6]. Finally, in order to preserve the accessible 6 DoF of the standard CTR, we propose the P2CuP2Cu which is a configuration with 2 concentric tubes augmented with 4 EAP electrodes each in order to control their bending in 2 orthogonal directions added to their telescopic deployment.

2.2 Forward kinematic model

The forward kinematic model first describes a single section of a CTR considering its actuators. As the modeling is based on the constant arc assumption, an arc of circle in 3D is defined, following Figure 1b, by its curvature κ_j (inverse of the radius of curvature r_j), its length ℓ_j, and the angle of the plane in which it is located ϕ_j.

Thus, the transformation matrix from the arc origin to its tip is:

$$^{j-1}T_j = T(\phi_j)T(\kappa_j,\ell_j) = \begin{bmatrix} R_z(\phi_j) & 0 \\ 0 & 1 \end{bmatrix} \begin{bmatrix} R_y(\theta_j) & \mathbf{p_j} \\ 0 & 1 \end{bmatrix} \tag{1}$$

where $\theta_j = \kappa_j \ell_j$ is the bending angle and $\mathbf{p_j} = [r_j(1-\cos\theta_j), 0, r_j \sin\theta_j]^T$. The arc variables are directly linked to the robot actuators, depending on the overlapping of the n tubes constituting m sections. For the considered P2CuP2Cu with 2 tubes, the actuator space is constituted of $\mathbf{q} = [V_{1x}\ V_{1y}\ V_{2x}\ V_{2y}\ \rho_1\ \rho_2]^T$ where $V_{ix,y}$ is the supplied voltage to the i^{th} tube according to its x and y axes respectively, and ρ_i is its translation for $i = \{1,2\}$. The intrinsic curvatures of each tubes are denoted $\kappa_{ix,y_{in}} = C_{EAP_i} V_{ix,y}$ noting that C_{EAP_i} is the EAP electro-chemical constant of the i^{th} tube electrodes. The intrinsic arc variables for the 2 tubes ($i = \{1,2\}$) are given by:

$$\begin{cases} \kappa_{i_{in}} = \sqrt{\kappa_{ix_{in}}^2 + \kappa_{iy_{in}}^2} \\ \phi_{i_{in}} = atan2(\kappa_{iy_{in}}, \kappa_{ix_{in}}) \end{cases} \tag{2}$$

The second section (containing only tube 2) variables are directly identified as $\kappa_2 = \kappa_{2_{in}}$ and $\phi_2 = \phi_{2_{in}}$. However, for the first section subject to the mechanical interaction of 2 tubes, one must compute the first section variables by:

$$\begin{cases} \kappa_1 = \sqrt{\kappa_{1x}^2 + \kappa_{1y}^2} \\ \phi_1 = atan2(\kappa_{1y}, \kappa_{1x}) \end{cases} \tag{3}$$

where $\kappa_{1x} = \dfrac{\sum_{i=1}^{2} E_i I_i \kappa_{i_{in}} \cos\phi_{i_{in}}}{\sum_{i=1}^{2} E_i I_i}$, and $\kappa_{1y} = \dfrac{\sum_{i=1}^{2} E_i I_i \kappa_{i_{in}} \sin\phi_{i_{in}}}{\sum_{i=1}^{2} E_i I_i}$. where κ_{ix} and κ_{iy} are the decomposition of the main curvature along the x and y axes respectively for the j^{th} section, E_i is the elastic modulus, and I_i is the cross sectional moment of inertia of the i^{th} tube. We should note that $\kappa_{i_{in}}$ is constant for the standard CTR when they are directly accessible in the proposed P2CuP2Cu with the pair of electrodes. Finally, considering the initial pose of the robot where all the tubes are withdrawn, the link lengths are such that $\ell_j = 0, \forall j = \{1,2\}$. Whenever the tubes are deployed, the link lengths are computed as $\ell_1 = \rho_1$ and $\ell_2 = \rho_2 - \rho_1$.

3 A geometrical approach to kinematic model inversion for 3T-1R planning

3.1 Model inversion

The model is inverted geometrically in order to find a closed-form expression and to properly control the robot end-effector position and orientation. For standard CTR

with 3 tubes, straightforward computation of the exact inverse kinematic model is not possible due to the non-linear equations involved and require challenging inverse kinematics or heuristic methods which are often limited by singularity issues, demand significant computational resources and a consequent execution time. In summary, the proposed algorithm computes the inverse kinematic model of the P2CuP2Cu in 3D for 4 DoF including the three position components and one in-plane orientation as described below.

Step I: Recalling the geometrical description of a tube in Figure 1b, we consider the robot sections that lie in the same plane Π where $\Pi = (O, \overrightarrow{z_0}, \overrightarrow{OB})$ is computed such that it includes the robot origin, the first section tangent at that origin ($\overrightarrow{z_0} = \overrightarrow{z_1}$), and the desired end-effector position respectively. The output of this step are the angles $\phi_1 = \phi_2$ describing the plane Π such as in equation 4.

$$\phi_j = atan2(Y_{end}, X_{end}), \tag{4}$$

Step II: Let us state that although the desired point is expressed in 3D, the process is performed in a 2D-way once the plane Π is figured out, and thus reduces substantially the computation complexity. The desired point is projected onto the plane Π such that its coordinates are ${}^{\Pi}X_{end} = \sqrt{X_{end}^2 + Y_{end}^2}$, ${}^{\Pi}Y_{end} = 0$, and ${}^{\Pi}Z_{end} = Z_{end}$. In all cases, the end-effector of an arc of a circle in the space is described in its base frame as in Figure 1b by equations 5 and 6.

$$\kappa_j = \frac{2\,{}^{\Pi}X_{end}}{{}^{\Pi}X_{end}^2 + {}^{\Pi}Z_{end}^2}, \tag{5}$$

$$\ell_j = \begin{cases} \frac{1}{\kappa_j}\, acos\left(1 - \kappa_j\, {}^{\Pi}X_{end}\right) & \text{if} \quad {}^{\Pi}Z_{end} > 0 \\ \frac{1}{\kappa_j}\left(2\pi - acos\left(1 - \kappa_j\, {}^{\Pi}X_{end}\right)\right) & \text{else.} \end{cases} \tag{6}$$

For the considered 2-tubes P2CuP2Cu, this single-arc inverse kinematic model is computed for each arc separately. Both arcs meet in A which is the inflection point along the robot structure. Let us assure that A lies in the aforementioned plane Π.

Step III: The position of A in the segment $[OB]$ defines the ratio L_r of the distances OA and AB and gives a global approximation of the arc lengths ℓ_1 and ℓ_2 ratio. This ratio can be changed considering the global design or the actuator constraints such as for translation motors used which may likely be set at their middle travel range for a safety purpose $L_r = 1$. For the first arc, considering its basis frame $(O, \overrightarrow{x_1}, \overrightarrow{y_1}, \overrightarrow{z_1})$, its variables κ_1 and ℓ_1 are computed for any point $A \in [OB]$ through equations 5 and 6 where the arc tangent at the origin O is $\overrightarrow{z_1}$.

Step IV: We solve for the same single-arc computation (Figure 1b with equations 5 and 6) such as the origin is point A, the arc tangent is $\overrightarrow{z_2}$ (which ensures the continuity in the robot shape), and the desired point B coordinates are expressed in the frame $(A, \overrightarrow{x_2}, \overrightarrow{y_2}, \overrightarrow{z_2})$ using the inverse transformation matrix of ${}^{0}T_1$. This leads

to the second arc variables κ_2 and ℓ_2.

Step V: Once the arc variables $\chi = [\kappa_1 \ \phi_1 \ \kappa_2 \ \phi_2 \ \ell_1 \ \ell_2]^T$ are computed, the actuator configurations $\mathbf{q}$ are calculated by inverting equations 2 and 3. For the brevity of this paper, such computations are not detailed.To check the validity of this solution, it is fed through the forward kinematic model to draw the robot shape and pose. The end-effector position must match the initial desired point as described in Figure 2a with orientation z_3.

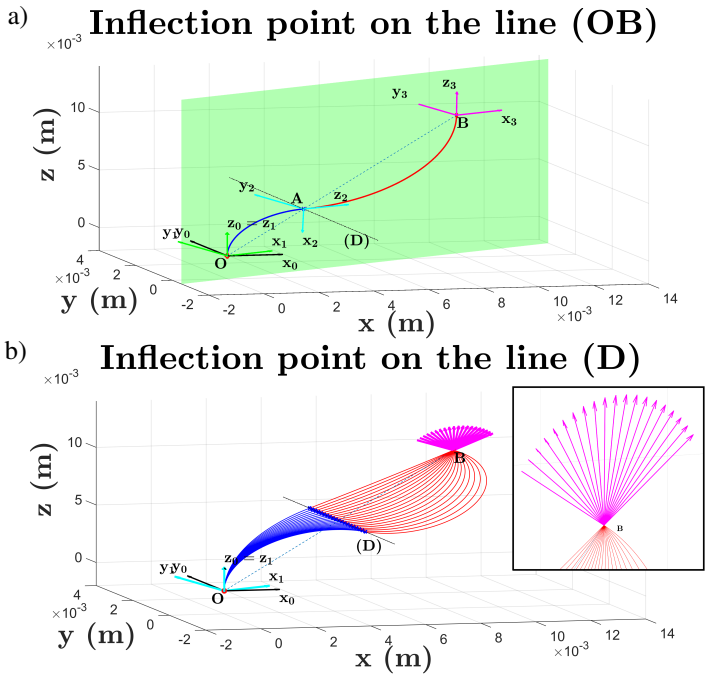

Fig. 2 Sliding the inflection point A a) on the line (OB) producing an arc length ratio L_r and b) then on the perpendicular (D) to (OB) in the plane Π at A after choosing a specific L_r.

Step VI: To obtain a different orientation of the end-effector $(B, \overrightarrow{z_3})$ in the plane Π, the perpendicular line (D) to (OB) in the plane Π at A is calculated. When sliding the point A on (D) and computing **steps (II) to (V)** to draw the robot shape, the orientation α of the vector $\overrightarrow{z_3}$ at B with respect to $\overrightarrow{z_1}$ is changed. This orientation is then proportional to the distance d of point A from (OB). The output of this step is this proportionality ratio Or_r such that $Or_r = \frac{\Delta d}{\Delta \alpha}$. An example of this step is depicted in Figure 2b (for a fixed ratio $L_r = 1$) where d varies up to $2mm$ on both sides of (D). The output orientations at B are shown where $Or_r = 32^\circ/mm$ and $\alpha \in [-60^\circ; 60^\circ]$.

Step VII: This calculated ratio Or_r is used to solve for all the desired in-plane orientations $\overrightarrow{z_3}^*$. In fact, from the calculated distance d, we obtain a new position of the inflection point A and the process is browsed again from **step (II) to step (V)** with a less complex **step (III)** as the point A is already defined. The algorithm returns the final actuator configuration $\mathbf{q_{final}} = [V_{1x}\ V_{1y}\ V_{2x}\ V_{2y}\ \rho_1\ \rho_2]^T$ in order to obtain the desired position B and orientation $\overrightarrow{z_3}^*$. The proposed solution considers in-plane orientations only and a more rigorous choice of the inflection point position in the space is an open topic for future work.

3.2 3T-1R task planning

Using the aforementioned kinematic inversion, examples of the path planning simulations of the P2CuP2Cu are presented hereby. For the intended medical applications, a sweeping scheme of the distal tube end-effector housing an optical imaging system (camera with fiber bundle, OCT probe, confocal microscope) is developed. More specifically, a square sweeping of 10x10mm is validated by the simulations in Figure 3a. One can note that the end-effector orientation is preserved (orthogonal to the examined tissue surface) which respects the constraints of a sweeping procedure. A circular path on a sphere of 2mm radius is also performed (Figure 3b) while keeping the orientation pointing to the sphere center as for a tissue examination with a sub-degree precision. These planning schemes were performed according to mechanical and fabrication constraints of a maximum arc lengths of 40mm and maximum curvatures of $200m^{-1}$.

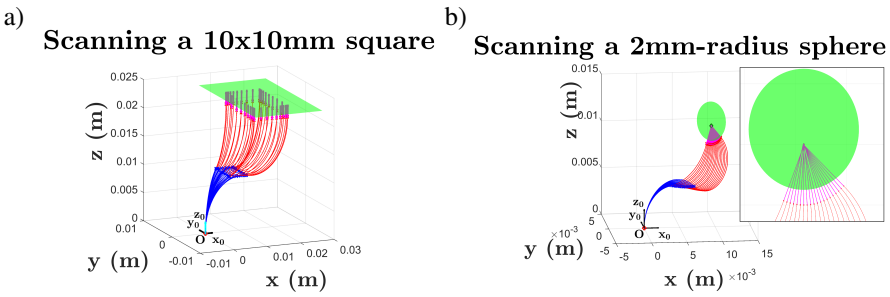

Fig. 3 For an arc length ratio $L_r = 1$, the robot poses during model inversion based path planning are shown for a) a square scanning and b) a spherical cap scanning schemes.

4 Conclusions

An alternative structure to the usual 3-tubes CTR was presented in this paper. This P2CuP2Cu is based on EAP micro-actuators and provides equivalent kinematic performances with only 2 tubes with a free lumen and a continuum shape approach. The major expected advantages of our robot are the compactness due to the embedded micro-actuation and the controllability especially for medical applications. Furthermore, the inverse kinematic model was analyzed in a geometrical approach and path planning schemes (namely tissue scanning) were validated in simulations for 3T-1R tasks. Deriving the complete inverse kinematic model is a future challenge and will conduct to a full pose control.

Acknowledgements This work has been supported by the Labex ACTION project (contract ANR-11-LABX-0001-01) and by NEMRO project (contract ANR-14-CE17-0013).

References

1. Barrand, L., Chikhaoui, M.T., Cot, A., Rabenorosoa, K., Rougeot, P., Lakard, B., Lakard, S., Andreff, N.: Towards polypyrrole actuated flexible endomicroscope: Synthesis. In: French Symposium on Emerging Technologies for Micro-Nanofabrication. Lyon, France (2015)
2. Burgner, J., Rucker, D., Gilbert, H., Swaney, P., Russell, P., Weaver, K., Webster, R.: A telerobotic system for transnasal surgery. IEEE/ASME Transactions on Mechatronics **19**(3), 996–1006 (2014). DOI 10.1109/TMECH.2013.2265804
3. Burgner, J., Swaney, P.J., Rucker, D.C., Gilbert, H.B., Nill, S.T., P. T. Russell, I., Weaver, K.D., Webster III, R.J.: A bimanual teleoperated system for endonasal skull base surgery. In: IEEE/RSJ International Conference on Intelligent Robots and Systems, pp. 2517–2523. San Francisco, USA (2011)
4. Burgner-Kahrs, J., Rucker, D., Choset, H.: Continuum robots for medical applications: A survey. IEEE Transactions on Robotics **31**(6), 1261–1280 (2015). DOI 10.1109/TRO.2015.2489500
5. Butler, E.J., Hammond-Oakley, R., Chawarski, S., Gosline, A.H., Codd, P., Anor, T., Madsen, J.R., Dupont, P.E., Lock, J.: Robotic neuro-endoscope with concentric tube augmentation. In: IEEE/RSJ International Conference on Intelligent Robots and Systems, pp. 2941–2946. Vilamoura, Portugal (2012)
6. Camarillo, D.B., Milne, C.F., Carlson, C.R., Zinn, M.R., Salisbury, J.K.: Mechanics modeling of tendon-driven continuum manipulators. IEEE Transactions on Robotics **24**(6), 1262–1273 (2008)
7. Chikhaoui, M.T., Rabenorosoa, K., Andreff, N.: Kinematic modeling of an eap actuated continuum robot for active micro-endoscopy. In: J. Lenarčič, O. Khatib (eds.) Advances in Robot Kinematics, pp. 457–465. Springer International Publishing (2014). DOI 10.1007/978-3-319-06698-1_47
8. Chikhaoui, M.T., Rabenorosoa, K., Andreff, N.: Towards clinical application of continuum active micro-endoscope robot based on eap actuation. In: Surgetica. Chambéry, France (2014)
9. Dupont, P.E., Lock, J., Itkowitz, B., Butler, E.: Design and control of concentric-tube robots. IEEE Transactions on Robotics **26**, 209–225 (2010)
10. Gosline, A.H., Vasilyev, N.V., Veeramani, A., Wu, M., Schmitz, G., Chen, R., Arabagi, V., del Nido, P.J., Dupont, P.E.: Metal mems tools for beating-heart tissue removal. In: IEEE International Conference on Robotics and Automation, pp. 1921–1926. Saint Paul, USA (2012)

11. Hendrick, R.J., Herrell, S., Webster III, R.J.: A multi-arm hand-held robotic system for transurethral laser prostate surgery. In: IEEE International Conference on Robotics and Automation, pp. 2850–2855. Hong Kong, China (2014). DOI 10.1109/ICRA.2014.6907268
12. Neppalli, S., Csencsits, M.A., Jones, B.A., D.Walker, I.: Closed-form inverse kinematics for continuum manipulators. Advanced Robotics **23**, 2077–2091 (2009)
13. Rucker, D.C., Croom, J.M., Webster III, R.J.: Aiming a surgical laser with an active cannula. Journal of Medical Devices **3**(2), 027,506 (2009)
14. Webster III, R.J.: Design and mechanism of continuum robot for surgery. Ph.D. thesis, The John Hopkins University, USA (2007)
15. Webster III, R.J., Romano, J.M., Cowan, N.J.: Kinematics and calibration of active cannulas. In: IEEE International Conference on Robotics and Automation, pp. 3888–3895. Pasadena, USA (2008). DOI 10.1109/ROBOT.2008.4543808
16. Xu, R., Asadian, A., Naidu, A., Patel, R.: Position control of concentric-tube continuum robots using a modified jacobian-based approach. In: Robotics and Automation (ICRA), 2013 IEEE International Conference on, pp. 5813–5818 (2013). DOI 10.1109/ICRA.2013.6631413